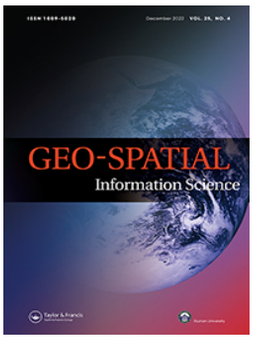

Geo-spatial Information Science

ISSN: (Print) (Online) Journal homepage: https://www.tandfonline.com/loi/tgsi20

Ground-based remote sensing of nitrous oxide (N_2O) over Hefei, eastern China from high-resolution solar spectra

Youwen Sun, Hao Yin, Wei Wang, Changgong Shan & Cheng Liu

To cite this article: Youwen Sun, Hao Yin, Wei Wang, Changgong Shan & Cheng Liu (2023): Ground-based remote sensing of nitrous oxide (N_2O) over Hefei, eastern China from high-resolution solar spectra, Geo-spatial Information Science, DOI: 10.1080/10095020.2023.2208616

To link to this article: https://doi.org/10.1080/10095020.2023.2208616

Published online: 01 Jun 2023.

GEO-SPATIAL INFORMATION SCIENCE
https://doi.org/10.1080/10095020.2023.2208616

Ground-based remote sensing of nitrous oxide (N_2O) over Hefei, eastern China from high-resolution solar spectra

Youwen Sun [a], Hao Yin [a,b], Wei Wang [a], Changgong Shan [a] and Cheng Liu [a,b]

[a]Anhui Institute of Optics and Fine Mechanics, HFIPS, Chinese Academy of Sciences, Hefei, China; [b]Department of Precision Machinery and Precision Instrumentation, University of Science and Technology of China, Hefei, China

ABSTRACT

We for the first time demonstrate ground-based remote sensing of Nitrous Oxide (N_2O) over Hefei in eastern China from high resolution Fourier Transform Infra-Red (FTIR) solar spectra. We have retrieved Column-averaged Abundance of N_2O (X_{N_2O}) from both Near-Infrared (NIR, 4000 to 11,000 cm^{-1}) and Mid-Infrared (MIR, 2400 to 3200 cm^{-1}) solar spectra and inspected their agreement. Generally, NIR and MIR measurements agree well with a correlation coefficient of 0.86 and an average difference of (1.33 ± 4.05) ppbv (NIR – MIR). By correcting the bias of the two datasets, we combine the NIR and MIR measurements to investigate seasonality and inter-annual trend of X_{N_2O} over Hefei. The observed monthly mean time series of X_{N_2O} minimize in June and maximize in September, with values of (316.55 ± 12.22) ppbv and (322.05 ± 12.93) ppbv, respectively. The X_{N_2O} time series from 2015 to 2020 showed an inter-annual trend of (0.53 ± 0.10) %/year over Hefei, China. We also compared the FTIR X_{N_2O} observations with GEOS-Chem model X_{N_2O} simulations. They are in reasonable agreement with a correlation coefficient (R) of 0.71, but GEOS-Chem model underestimated the seasonality of the observations. This study can enhance current knowledge of ground-based high-resolution FTIR remote sensing of N_2O in the atmosphere and contribute to generating a new reliable N_2O dataset for climate change research.

ARTICLE HISTORY
Received 1 December 2022
Accepted 24 April 2023

KEYWORDS
Greenhouse Gases (GHGs); remote sensing; high resolution; Fourier Transform Infra-Red (FTIR)

1. Introduction

N_2O ranks as the third largest contributor to global warming (Stein and Yung 2003). In stratospheric atmosphere, N_2O is a significant anthropogenic driver of ozone depletion and a major source of Nitric Oxide (NO) (Nevison et al. 2011; Portmann, Daniel, and Ravishankara 2012; Ravishankara, Daniel, and Portmann 2009). N_2O is a very stable Greenhouse Gas (GHG) and it has a lifetime of about 114 years in the atmosphere (United States Environmental Protection Agency 2019). Globally averaged N_2O in 2016 relative to 1750 has increased by 22%, corresponding to an inter-annual increase trend of 0.7 to 1.0 ppbv/year (Machida et al. 1995; Prinn et al. 1990, 2000). On global scale, the source of N_2O is attributed to natural emissions by 60% and anthropogenic emissions by 40%. The sink of N_2O is mainly depleted by ultraviolet photolysis in the stratosphere (Morgan et al. 2004). Additional sink of N_2O is through photo oxidation with $O(^1D)$ to produce Nitrogen Oxides (NO_x) (Montzka, Dlugokencky, and Butler 2011). The Kyoto Protocol has included N_2O as one of the major GHGs targeted for emissions reduction (UNFCC 1997). Precise detection of the abundance and variability of N_2O is of great significance not only for understanding its source, transport, chemical mechanism, and thus establishing a scientific link between its variability and climate change, but also for improving theoretical Chemical Transport Models (CTMs) and potential control purposes.

Compared with in situ surface data, column observations pass through a larger portion of the atmosphere, resulting in a less temporal variability but still keeping information on surface fluxes (Wunch et al. 2011; Yin et al. 2019). As a result, the horizontal gradients of column observations are more associated with sources and sinks of underlying regional fluxes (Sun et al. 2020, 2018a, 2021a, 2021b). Ground-based high-resolution FTIR spectroscopy has been verified as one of the most precise remote sensing tools to derive total columns and Vertical Mixing Ratio (VMR) profile of N_2O. Both the Total Columns Carbon Observing Network (TCCON) and Network for Detection of Atmospheric Composition Change (NDACC) networks use high resolution FTIR spectrometers to monitor atmospheric N_2O abundance. The TCCON/NDACC networks initiated in 2004/1992 and a few stations have provided datasets of total columns and VMR profile of N_2O for more than 20

CONTACT Cheng Liu chliu81@ustc.edu.cn

years. The California Laboratory for Atmospheric Remote Sensing (CLARS) which is not afflicted with the TCCON/NDACC networks also uses high resolution FTIR spectrometer to observe the long-term variability of N_2O over the Los Angeles basin (Addington et al. 2021). The inter-annual trends of N_2O have been reported in different regions with ground-based high resolution FTIR observations. Angelbratt et al. (2011) estimated that N_2O inter-annual trends varied between (0.19 ± 0.01) and (0.40 ± 0.02) %/year in four European FTIR stations during 1996–2007. Zhou et al. (2019) have compared the abundance and inter annual trends of N_2O from the TCCON and NDACC observations at seven FTIR observation sites around the globe, and concluded that N_2O in these sites varied over (0.81 ± 0.04) to (0.93 ± 0.02) %/year during 2007–2017. Sagar et al. (2022) also retrieved CO_2, CH_4 and CO concentrations using ground-based EM27/SUN FTIR in India.

Historically, most FTIR sites are distributed in Northern America and Europe, but the number of sites in other parts of the world is very sparse. Currently, only two TCCON stations have been set up in China, the Hefei station in eastern China (117.2°E, 32.0°N) and the Xianghe station in northern China (116.96°E, 39.75°N) (Tian et al. 2017; Wang et al. 2017; Yang et al. 2020; Yin et al. 2021a). In this manuscript, we first retrieve and characterize the variability of atmospheric N_2O over the Hefei station by using high-resolution FTIR spectroscopy. The N_2O retrievals derived from high resolution NIR (4,000 to 11,000 cm^{-1}) and MIR (2,400 to 3,200 cm^{-1}) solar spectra are compared. Furthermore, the NIR and MIR measurements from 2015 to 2020 are combined to investigate seasonality and inter annual trend of X_{N_2O} over Hefei. In addition, a comparison between GEOS-Chem simulations and FTIR observations are also performed. This study can enhance current knowledge of ground-based high-resolution FTIR remote sensing of N_2O in the atmosphere and contribute to generate a new reliable N_2O dataset for climate change research.

2. Methodology

2.1. FTIR observation

2.1.1. Instrumentation

The operational FTIR observation site (117.2°E, 31.5°N, 30 m a.s.l. (above sea level)), run by the Anhui Institute of Optics and Fine Mechanics, Chinese Academy of Sciences (AIOFM-CAS), is located in the suburb of Hefei city (the capital city of Anhui Province) in central-eastern China. The downtown Hefei is located to the southeast of this site and is densely populated with eight million people. The site is surrounded by wetlands or cultivated lands in other directions. The anthropogenic emissions mainly come from the city and the natural emissions are originated from cultivated lands or wetlands. Routine observations at the site have been implemented since 2014. The observatory is currently the only site in China that has a continuously-operating solar FTIR, making it crucial to calibrate and validate the satellite data or model simulations in this important region.

The observatory at Hefei includes a high-resolution FTIR spectrometer, a solar tracker, and a weather station. The FTIR spectrometer is installed inside a room, while the solar tracker and the weather station are placed on the roof of the room. The IFS125HR spectrometers show outstanding capabilities such as the accuracy and stability, and have been extensively applied within the TCCON/NDACC networks (Sun et al. 2021a, 2021b; Yin et al. 2020, 2021a, 2022b). The IFS125HR spectrometer at the Hefei site includes four beam splitters, nine optical path compartments, and six detectors. This spectrometer covers a wide wavenumber range of 400 to 50,000 cm^{-1} with a maximum spectral resolution of 0.001 cm^{-1}. With the state-of-the-art Camtracker mode, the solar tracker captures and guides solar beam uninterruptedly into the FTIR spectrometer with a precision of ±0.1 mrad (Hall et al. 2011). The meteorological station includes sensors for relative humidity (±3.0%), air temperature (±0.30°C), air pressure (±0.1hpa), solar radiation (±5.0%), wind speed (±0.40 m/s), and wind direction (±4.0°) (Sun et al. 2018a, 2017). These meteorological data are applied for retrievals or source attribution of the measurements.

In present work, we equip the FTIR spectrometer with a CaF_2 beam splitter and an InGaAs detector for N_2O observations in the NIR range (4000–11,000 cm^{-1}) and a KBr beam splitter, a filter with a center wavenumber of 2800 cm^{-1}, and an InSb detector for N_2O observations in the MIR range (2400–3100 cm^{-1}). We restricted the entrance aperture size to be 1 mm for all NIR measurements, while a size varying from 0.10 to 2.5 mm was implemented for the MIR measurements. Entrance aperture implemented in this manner can maximize the signal-to-noise ratio (SNR) while retaining unsaturated signals. The NIR and MIR solar spectra are saved alternatively during routine operations. The number of NIR and MIR N_2O observations within a sunny day range from 1 to 48.

2.1.2. Retrieval and characterization of N_2O in the NIR range

We utilize the GGG version 2020 to retrieve N_2O total columns from NIR solar spectra. GGG (Wunch et al. 2011) is a TCCON standard software which operates a suite of software package to retrieve total columns of various gaseous constituents from FTIR solar spectra. In order to obtain a site-to-site consistency of the retrievals, a same version of software is mandatorily

used for all TCCON sites (Wunch et al. 2015). The GGG first operates a subroutine procedure of interferogram-to-spectrum (I2S) to convert the interferograms into spectra. A subroutine procedure of "GSETUP" is then operated to generate *a priori* profiles of N_2O and other trace gases. Meanwhile, *a priori* profiles of temperature, pressure, and H_2O are straightly interpolated from the NCEP/NCAR reanalysis. This subroutine procedure takes into account a series of issues, including an interhemispheric gradient, a secular increase, stratospheric decay, and seasonal cycle. Finally, a subroutine procedure called the nonlinear least-squares fitting algorithm "GFIT" scales iteratively the a priori profiles to produce calculated spectra until the best fit to the measured spectra. The total columns of N_2O (T_{N_2O}) is thus calculated via Equation (1).

$$T_{N_2O} = \int_{z_s}^{z_{top}} A_m(z) \times f_{N_2O}(z) dz, \quad (1)$$

where f_{N_2O} (z) represents the integral of the mole fraction of N_2O, A_m(z) is air-mass profile. The upper and lower limits of the integration, z_{top} and z_s, denote the top of atmosphere (TOA) and the surface, respectively. Unlike total columns which is affected by topography and surface pressure, column-averaged abundance has a low sensitivity to fluctuations of surface pressure and H_2O. This characteristic allows direct comparisons of column observations with in situ data in different seasons and thus is advantageous for atmospheric cycle investigations (Wunch et al. 2015). T_{N_2O} can be converted into column-averaged abundance of N_2O (X_{N_2O}) via Equation (2). Taking the ratio in Equation (2) minimizes the systematic errors which are common to N_2O and O_2.

$$X_{N_2O} = \frac{T_{N_2O}}{T_{air}} = \frac{T_{N_2O}}{T_{O_2}} \times 0.2095 \quad (2)$$

where T_{air} and T_{O_2} are total columns of dry air and O_2, respectively. Input parameters and setups for N_2O and O_2 retrievals from NIR spectra using GGG version 2020 are summarized in Table 1 (Kalnay et al. 1996). As described in Wunch et al. (2011) and Wunch et al. (2015), N_2O is retrieved in three spectral micro windows (MWs: 4373.5–4416.9 cm^{-1}, 4418.55–4441.65 cm^{-1} and 4682.95–4756.05 cm^{-1}), and O_2 is retrieved in the spectral window of 7765.0–8004.0 cm^{-1}. The cross-interferences of H_2O, CO_2, and HF are considered in the O_2 window and the cross-interferences of CH_4, H_2O, HDO and CO_2 are considered in the N_2O window. Spectroscopic parameters of all gases are extracted from the HITRAN 2020 database (Hill et al. 2013; Rothman et al. 2009).

We collect and retrieve NIR spectra at Hefei following the TCCON recommendation, and thus the error budget for N_2O by the TCCON community could also apply to Hefei observations. Wunch et al. (2011) perturbed each potential error by a realistic amount in the GGG forward model and calculated the relative difference in X_{N_2O} relative to the unperturbed case. This sensitivity study was proceeded with solar spectra collected on a clear day at the Lamont site, which spanned a large difference in H_2O, temperature, and solar zenith angle (SZA). The total error is estimated as the sum in quadrature of all potential errors. According to Wunch et al. (2015), the total errors of X_{N_2O} are ~1% and reasonably independent of SZA. The dominant error sources are shear misalignment, a priori profile shape, observer-sun Doppler stretch (OSDS), and zero level offsets. At high SZAs, the a priori temperature profile and pointing offsets become significant. The *a priori* profile and the column AVK for X_{N_2O} retrieval at Hefei in the NIR range are presented in Figure 1(a,b), respectively. The results show that the sensitivity of X_{N_2O} retrieval at Hefei in the NIR range decreases as the SZAs increases, but all sensitivities are greater than 0.5 between surface and 70 km. It means that more than 50% of retrieval information comes from observation, i.e. the *a priori* information affects the retrieval by less than 50% in both troposphere and stratosphere. It also indicates that the NIR observations for N_2O at Hefei are sensitive to both troposphere and stratosphere regardless of SZAs.

2.1.3. Retrieval and characterization of N_2O in the MIR range

We use the SFIT4 software to retrieve N_2O from MIR spectra. Inputs and setups of the SFIT4 follow the

Table 1. Input parameters and setups for N_2O and O_2 retrievals from NIR solar spectra.

Species	N_2O	O_2
Retrieval Code	GGG2020	GGG2020
Spectroscopy	HITRAN 2020	HITRAN 2020
A priori profiles of temperature and pressure	NCEP	NCEP
A priori profiles of gases	GGG2020 code	GGG2020 code
Micro windows (cm^{-1})	4373.5–4416.9 4418.55–4441.65 4682.95–4756.05	7765–8005
Micro spectral window width (cm^{-1})	43.4 23.1 73.1	240
Retrieved interfering species	CH_4, H_2O, CO_2, HDO	CO_2, H_2O, HF

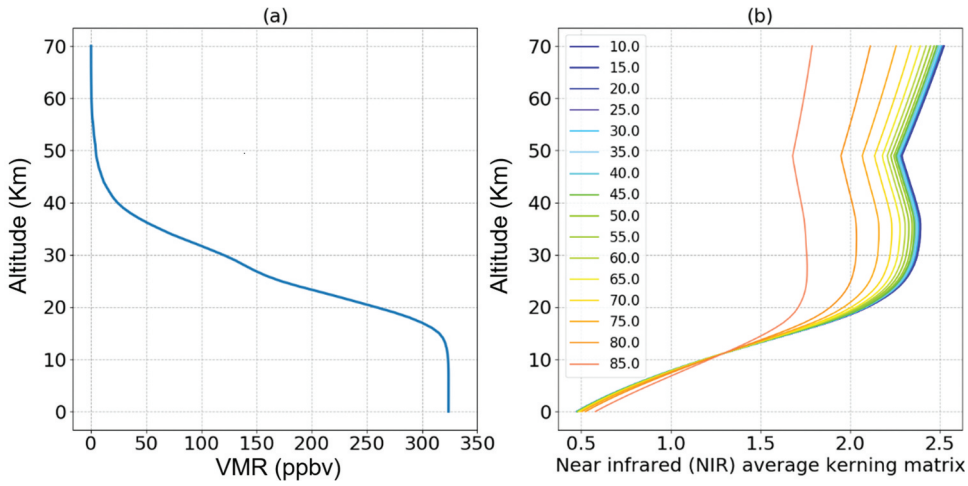

Figure 1. (a) The a priori profile of N_2O used in NIR spectra retrieval. (b) Averaging kernel (AVK) matrix for N_2O retrieval with GGG2020.

NDACC recommendation and are tabulated in Table 2. We take monthly mean profiles of WACCM model simulations between 1980 and 2020 as the *a priori* profiles of all gases (not including H_2O). The a priori profiles of meteorological parameters such as Temperature, humidity, and Pressure are straightly taken from NCEP/NCAR reanalysis (Kalnay et al. 1996). Three MWs of 2441.8–2444.6 cm^{-1}, 2481.2–2482.5 cm^{-1} and 2806.05–2806.55 cm^{-1} were used to retrieve N_2O profiles. CH_4, HDO, and H_2O show absorption interference with N_2O in all retrieval windows. In addition to N_2O profile, we also retrieve total columns of CH_4 and HDO, and H_2O profile in the same MWs to minimize the cross absorption interferences. The spectroscopic parameters of all gases are extracted from the HITRAN 2020 database, which is same as the NIR spectra retrievals (Hill et al. 2013; Rothman et al. 2009).

To regularizing the retrieval, we set the diagonal values of the noise covariance matrix $\mathbf{S_\varepsilon}$ to be square inverse of the SNR of each spectrum, and its non-diagonal values to be zero. We set the diagonal values of *a priori* covariance matrices $\mathbf{S_a}$ to be covariance of WACCM simulations between 1980 and 2020, and their non-diagonal values to be zero. In order to avoid inconsistencies in the total columns due to optical misalignment, we use the true instrumental line shape (ILS) derived from regular low-pressure HBr cell measurements to retrieve the time series of N_2O. (Hase 2012; Hase, Blumenstock, and Paton-Walsh 1999; Sun et al. 2018a, 2018b).

The AVK matrix **A** characterizes vertical information of the retrieval. The trace of **A** is called the degrees of freedom for signal (DOFS), which indicates that how much independent information can be derived

Table 2. Inputs and setups for N_2O retrieval from MIR spectra at Hefei.

Gases		N_2O
Code		SFIT4
A priori profiles for all gases (not including H_2O)		Statistics of WACCM simulations
A priori profiles of Temp., Humid., and Pres.		NCEP
Spectroscopy		HITRAN2016
Micro-widows (cm^{-1})		2441.8–2444.6 2481.2–2482.5 2806.05–2806.55
Micro spectral window width (cm^{-1})		2.8 1.3 0.5
Retrieved interfering gases		CH_4, CO_2, HDO
Regularization	S_ε	Real SNR (calculated in the actual observation in each spectrum)
	S_a	Covariance of WACCM simulation
ILS		measured
Error (2.20%)		Random error: (1.18%) -measurement error (measurement) -interference errors: interfering gases (interfering_species), retrieval parameters (retrieval_parameters) -other errors: zero level (zshift), Temp. (temperature) Systematic error: (1.86%) -smoothing error (smoothing) -other errors: optical path difference (max_opd), spectral curvature (curvature), solar strength (solstrnth), field of view of incident solar beam (omega), shift of solar line (solshft), background slope (slope), solar zenith angle (sza), phase (phase), pressure induced line broadening (linepair_gas), temperature induced line broadening (linetair_gas), intensity of spectroscopic line (lineint_gas)

from the retrieval. The area of **A** represents the retrieval sensitivity at each layer. Figure 2 demonstrates the a priori and retrieved VMR profiles of N_2O (a), cumulative sum of DOFS (b), and the AVKs (c) for N_2O retrieval randomly selected in the MIR range. Ground-based FTIR N_2O retrievals in the MIR range at Hefei has a DOFS of 2.0 from surface to 12 km and 2.1 from 12 km to 40 km, which means that the MIR retrievals are sensitive in both troposphere and stratosphere. Typical DOFS over the total atmosphere for N_2O retrievals in the MIR range is 4.1, indicating that we can obtain almost four independent information on the retrieved VMR profile. Therefore, the N_2O total columns and X_{N_2O} discussed in this study are reliable. The N_2O total columns is obtained by integrating the N_2O profile from ground to the TOA. The X_{N_2O} is then obtained by a weighting average of the air mass and the N_2O profile from ground to the TOA. Figure 2 shows that the retrieved profile deviates slightly from the *a priori* profile and is weighted for both troposphere and stratosphere due to the higher DOFS.

Error analysis for N_2O retrievals in the MIR range at Hefei follows the methodology of Rodgers (2000). We classified each individual error source as random or systematic error depending on if it varies randomly or is constant over observation. In present work, the random errors include *z*-shift error, measurement noise, and uncertainties of interfering species temperature, and retrieval parameters. The systematic errors include uncertainties of optical path difference, background curvature, solar line shift, the field of view of the incident solar beam, interferogram phase, the strength of solar line, pressure induced line broadening, temperature induced line broadening, and spectroscopic line intensity. Table 2 concludes the random, systematic, and total error for the N_2O retrieval exemplified in Figure 3. The input covariance matrix of observation noise was set to be the inverse square of the SNR of each spectrum and the temperature was estimated to be 2–7 K in the profile. The input covariance matrix of each interfering species was based on the WACCM climatology between 1980 and 2020. The input covariance matrix of field of view, background curvature, interferogram phase, optical path difference, shift of solar line, and strength of solar line were estimated to be 0.1%. The input covariance matrix of smoothing error and each retrieval parameter were obtained straightly from SFIT4 output. Spectroscopic uncertainties of spectroscopic line intensity, temperature, and pressure induced broadening coefficients for N_2O in the HITRAN 2020 line-list database were estimated to be 2%.

As shown in Figure 3, for N_2O retrieval in the MIR range at Hefei, the largest random error and systematic error are smoothing uncertainty (1.12%) and line intensity uncertainty (1.66%), respectively. Total error estimated as the sum in quadrature of total random errors (1.18%) and systematic errors (1.86%) is 2.20%.

2.1.4. Data filter criteria

We established a series of filter criteria to exclude the outliers that are heavily impacted by unstable weather conditions. Observations satisfying all the following criteria were regarded as valid observations and were applied in subsequent analysis, which excluded 23.4% of total observations.

(1) Auxiliary data such as solar flux, surface temperature, humidity, and pressure must be collected synchronously with the observations.

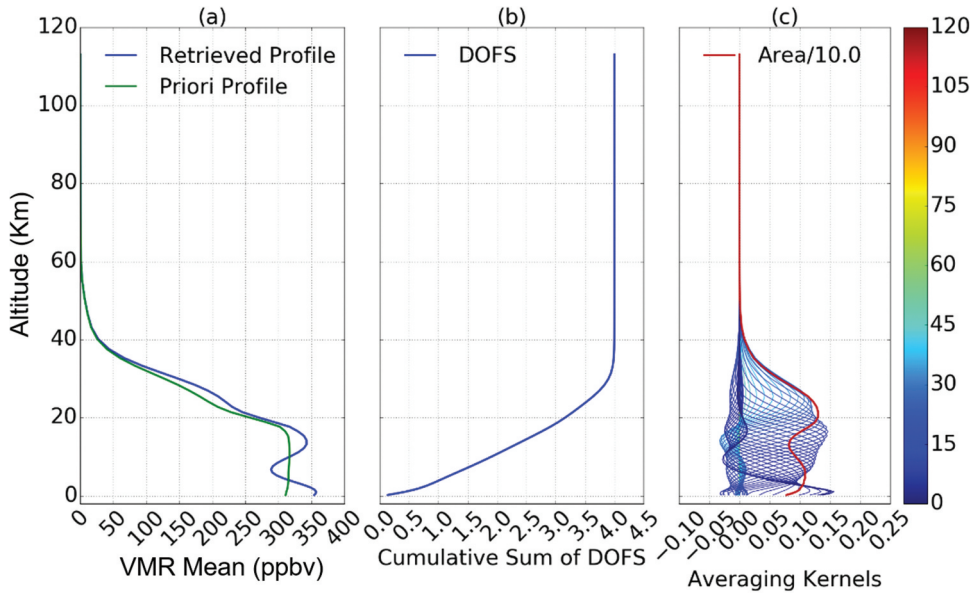

Figure 2. (a) The a priori and retrieved profiles of N_2O, (b) cumulative sum of DOFs for N_2O retrieval, (c) the AVK matrix A and their area. The demonstrations are randomly selected N_2O retrieval in the MIR range.

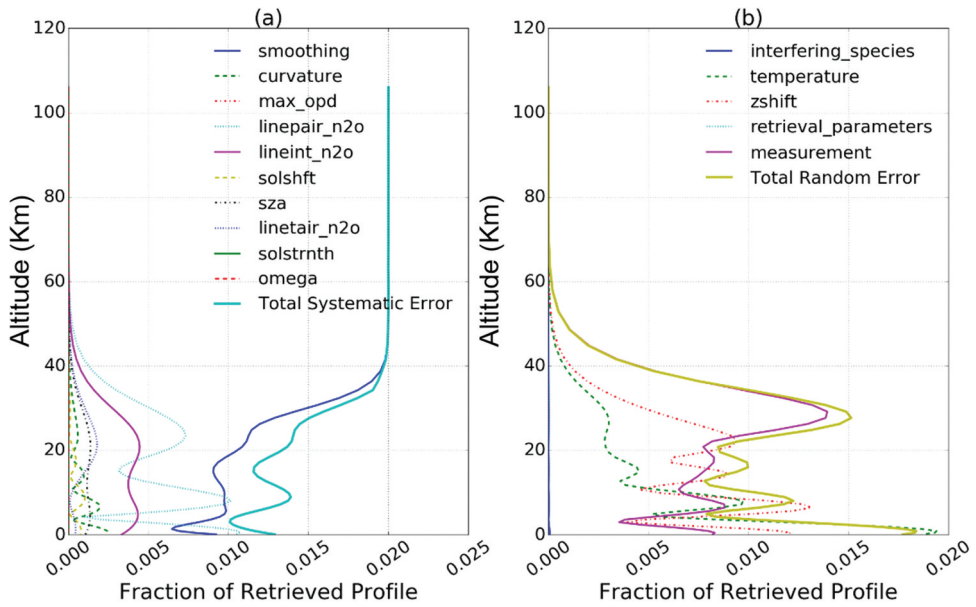

Figure 3. (a) Systematic error budgets for N_2O retrievals in the MIR range. (b) Same as (a) but for random error budgets. Descriptions of the error components inside each panel are listed in Table 2.

(2) The signal intensities of NIR spectra much vary between 7,000 and 22,000 counts and those of MIR spectra must vary between 10,000 and 20,000 counts. These thresholds well balanced the SNR and the non-linearity in the detector.
(3) The observation scenario must be nearly cloud free. We reject any spectra which were saved when the variation of solar intensity is larger than 10%.
(4) For both NIR and MIR solar spectra, the SZA must be smaller than 80°.
(5) All retrievals must be converged and the concentrations at all vertical heights must be positive. For MIR spectra retrievals, the total DOFs must be greater than 3.0 to make sure that the retrieval at each partial layer comes more from observation.
(6) The root means square error (RMS) of the fitting residual has to be smaller than 3% for N_2O retrieval in the NIR range and 5% in the NIR range.

2.2. GEOS-Chem model

We use GEOS-Chem model v12.2.1 to simulate N_2O around the globe at a 2° latitude × 2.5° longitude spatial resolution and 72 vertical pressure levels. We refer to Yin et al. (2019) for detailed description of model configuration. Briefly, the GEOS-Chem model is operated in a standard mode and driven by the GEOS-FP meteorological field. In order to drive the GEOS-Chem model, the GEOS-FP with an original spatial resolution of 0.25°×0.3125° has been downgraded to 2°× 2.5°. The meteorological data has a vertical pressure resolution of 72 levels starting from ground to 0.015 hPa, and temporal resolutions of 1 h for surface meteorological elements and 3 h for other meteorological elements.

Global anthropogenic emissions of aerosol species (mainly black carbon and organic carbon) and gases (SO_2, NH_3, NO_x, CO, CH_4, NMVOCs, etc.) between 2015 and 2017 are based on the MIX inventory over Asia and the CEDS (Community Emissions Data System) inventory in other parts of the world (Hoesly et al. 2018). Biomass burning emissions of atmospheric species are coupled with the GFED4 (Global Fire Emission Database version 4) inventory (Giglio, Randerson, and Van Der Werf 2013). The UCX (Universal tropospheric-stratospheric Chemistry eXtension) chemical mechanism and the FAST-JX v7.0 photolysis algorithm are implemented, which includes a detailed "NO_x-O_x-hydrocarbon-aerosols" chemistry in the troposphere (Eastham, Weisenstein, and Barrett 2014). In stratosphere, bromine gases concentrations are based on climatology (Mclinden et al. 2000), ozone concentrations are estimated by the linearized ozone (Linoz) parameterization (Parrish et al. 2014), and other species concentrations are calculated by using archived monthly mean production s and loss rate from NASA's GMI scheme (Murray et al. 2012; Rothman et al. 2009).

3. Results and discussion

3.1. Comparisons between NIR and MIR observations

We compare N_2O retrievals in the NIR and MIR ranges at Hefei to inspect the agreement of these two datasets and to determine how they can be combined to evaluate the variability of N_2O. The

NIR and MIR solar spectra in present work were saved with the same instrument, but the optical components such as optical filter, beam-splitter and detector, and the retrieval strategies such as *a priori* profiles, spectroscopic MWs, and spectral iterative method are different, which could result in discrepancy in NIR and MIR N_2O retrievals. To properly compare the NIR and MIR N_2O retrievals, we use the methodology of Rodgers and Connor (2003) to conform their differences in *a priori* information and AVKs. Both NIR and MIR N_2O total columns associated with the *a priori* information and the true atmospheric state can be expressed as,

$$TC_r = TC_a + \boldsymbol{A}(PC_t - PC_a) + \varepsilon, \tag{3}$$

where $\boldsymbol{A}$ represents the AVKs associated with the NIR or MIR retrievals; PC_a and PC_t represent *a priori* and true N_2O partial columns, respectively; TC_r and TC_a represent retrieved and *a priori* N_2O total columns, respectively. The ε represents characterization error. Therefore, the discrepancy in N_2O total columns between MIR ($TC_{N_2O,MIR}$) and NIR ($TC_{N_2O,NIR}$) observations can be expressed as,

$$\begin{aligned} TC_{N_2O,NIR} - TC_{N_2O,MIR} = {} & (X_{NIR}^{apriori} - X_{MIR}^{apriori}) \\ & + (\boldsymbol{A}_{NIR} - \boldsymbol{A}_{MIR})X_{true} \\ & + (\boldsymbol{A}_{NIR}X_{NIR}^{apriori} \\ & - \boldsymbol{A}_{MIR}X_{MIR}^{apriori}), \end{aligned} \tag{4}$$

where $X_{\mathrm{NIR}}^{apriori}$ and $X_{\mathrm{MIR}}^{apriori}$ are a priori profiles of N_2O for NIR and MIR observations, respectively; X_{true} is the X_{N_2O} in the true atmospheric state; $\boldsymbol{A}_{\mathrm{NIR}}$ and $\boldsymbol{A}_{\mathrm{MIR}}$ are the AVKs of the retrievals in the NIR and MIR ranges, respectively. As a result, in addition to their different sensitivities of forward model to the real atmospheric state in different spectroscopic MWs, the discrepancy in N_2O total columns between MIR and NIR observations are dominated by the following two factors: (a) the difference in AVKs and (b) the difference in a priori profiles. To reconcile these differences, we use the methodology of Rodgers and Connor (2003) to project the NIR dataset into MIR retrieval scenarios. We first interpolate the NIR daily mean profiles of N_2O into the MIR vertical height to obtain a common height grid. We then use the a priori profiles to correct the interpolated NIR profiles by,

$$X_{NIR}^{'} = X_{NIR} + (\boldsymbol{A}_{NIR} - \boldsymbol{I})(X_{NIR}^{apriori} - X_{MIR}^{apriori}), \tag{5}$$

where $X_{\mathrm{NIR}}^{'}$ is a N_2O dataset that has been corrected by the a priori profile, X_{NIR} is the original NIR N_2O dataset, matrix $\boldsymbol{I}$ is the unity diagonal matrix. Finally, we further correct $X_{\mathrm{NIR}}^{'}$ using the smoothing function by,

$$X_{NIR}^{''} = X_{MIR}^{apriori} + A_{NIR}(X_{NIR}^{'} - X_{MIR}^{apriori}), \tag{6}$$

where $X_{\mathrm{NIR}}^{''}$ represents a N_2O dataset that has been corrected by *a priori* profile and smoothing function. This characteristic allows direct comparisons of column observations with in situ data in different seasons.

Following above procedures, all NIR N_2O data have been projected into MIR retrieval states and compared with the MIR data. Comparisons between daily mean NIR measurements and MIR measurements are shown in Figure 4. We can see in Figure 4 that NIR and MIR X_{N_2O} datasets are in good agreement, with an average difference of (1.33 ± 4.05) ppbv ($TC_{N_2O,NIR} - TC_{N_2O,MIR}$) and a correlation coefficient (R) of 0.86. Seasonal cycles of NIR and MIR X_{N_2O} data in Figure 5 shows that the largest difference of the two datasets occurs in August with a value of (−3.11 ± 5.36) ppbv and the lowest difference occurs in December with a value of (−0.36 ± 6.71) ppbv ($TC_{N_2O,NIR} - TC_{N_2O,MIR}$). The monthly mean differences between NIR and MIR X_{N_2O} data from 2015 to 2020 are within (1.40 ± 3.12) ppbv. Considering the X_{N_2O} amplitude is seasonal dependent, we also investigated the variation of the fractional difference between NIR and MIR datasets, which are deduced as the ratios of the absolute discrepancies ($TC_{N_2O,NIR} - TC_{N_2O,MIR}$) to the monthly mean values of the MIR dataset. The results show that the fractional differences of the two datasets are seasonal independent. Therefore, in present work, we first plus a mean bias of 1.4 ppbv to all NIR data and then combine the NIR and MIR datasets to evaluate the seasonal and inter annual variabilities of N_2O.

3.2. Seasonality and inter-annual trend

In Figure 6, we have used a second Fourier series plus a linear curve to fit the joint NIR+MIR daily mean time series of X_{N_2O}. Such fitting is based on Gardiner's bootstrap resampling methodology which has been

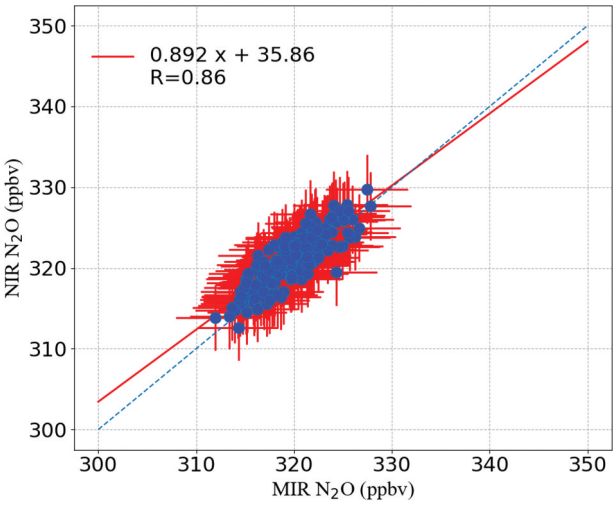

Figure 4. Comparisons between daily mean NIR X_{N_2O} measurements against MIR X_{N_2O} observations. The red line represents a linear fit to concurrent scatter points.

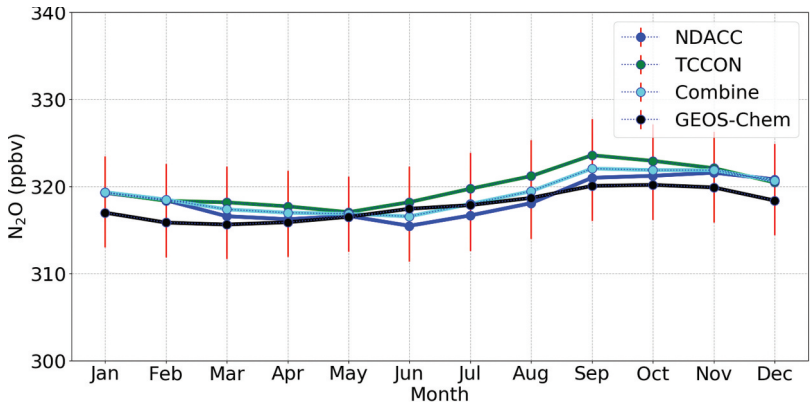

Figure 5. Monthly mean of NIR, MIR, joint NIR+MIR, and GEOS-Chem model X_{N_2O} data. The vertical error bars represent the 1-σ standard variations.

used in many studies to determine the seasonality and inter-annual trends of many constituents in the atmosphere (Sun et al. 2021c; Yin et al. 2019, 2020, 2021a, 2021b, 2022a). In present work, the measured daily mean time series of X_{N_2O} related to the regression model is formulated as Equation (7),

$$V(t,\mathbf{b}) = b_0 + b_1 t + b_2 \cos(\frac{2\pi t}{365}) + b_3 \sin(\frac{2\pi t}{365}) \quad (7)$$

$$F(t,\mathbf{b}) = V(t,\mathbf{b}) + \varepsilon(t) \quad (8)$$

$$d\% = \frac{F(t,\boldsymbol{b}) - V(t,\boldsymbol{b})}{V(t,\boldsymbol{b})} \times 100\%, \quad (9)$$

where $V(t,\boldsymbol{b})$ and $F(t,\boldsymbol{b})$ are the fitted and measured daily mean time series of X_{N_2O}, respectively. b_0, b_1, b_2, and b_3 are the bootstrap resampling regression coefficients fitted with the model $V(t,\boldsymbol{b})$. b_0 represents the intercept, b_1 is the annual change rate, and b_1/b_0 is the inter-annual trend discussed below. b_2 and b_3 characterize the seasonality, t represents the fractional of the year elapsed since the start year of the time series (i.e. 2015 in present work), and ε(t) is the difference between measured and fitted time series. Equation (9) that calculates the fractional differences of X_{N_2O} measurements relative to the monthly mean values of $F(t,\boldsymbol{b})$ is used to analyze seasonal enhancements.

The bootstrap resampling model can generally reproduce the measured seasonality and inter-annual trend of X_{N_2O} from 2015 to 2020 with an R of 0.81. Figure 5 showed clear seasonal characteristics of X_{N_2O} over Hefei: (1) high values of X_{N_2O} appear in the late summer to early winter and low values of X_{N_2O} appear in late winter to summer; (2) the variations in X_{N_2O} are seasonal-independent and relatively stable. (3) the seasonality of X_{N_2O} varies over a unimodal mode, i.e. the seasonal trough appears around June–July and the seasonal peak appears around September to November.

The joint NIR+MIR X_{N_2O} time series minimize in June and maximize in September, with values of (316.55 ± 12.22) ppbv and (322.05 ± 12.93) ppbv, respectively. The joint NIR+MIR X_{N_2O} measurements in September were on average (1.71 ± 5.22) % higher than those in June. The annual mean values of joint NIR+MIR X_{N_2O} over Hefei are (317.90 ± 5.04) ppbv, (318.41 ± 4.90) ppbv, (319.91 ± 4.11) ppbv, (319.74 ± 5.82) ppbv, (319.80 ± 6.21) ppbv, and (320.83 ± 3.78) ppbv in 2015, 2016, 2017, 2018, 2019, and 2020, respectively. The observed X_{N_2O} measurements from 2015 to 2020 showed a positive inter-annual trend of (0.53 ± 0.10) % per year (Figure 6). Depending on

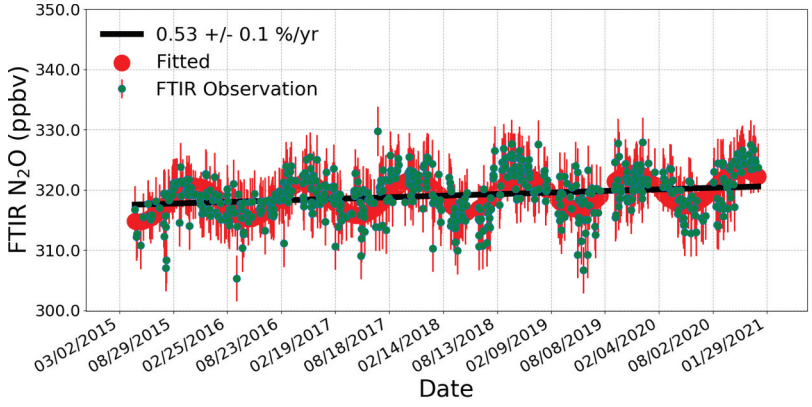

Figure 6. Daily mean time series of joint NIR + MIR X_{N_2O} measurements between 2015 and 2020 as well as the fitted seasonality and inter-annual trend.

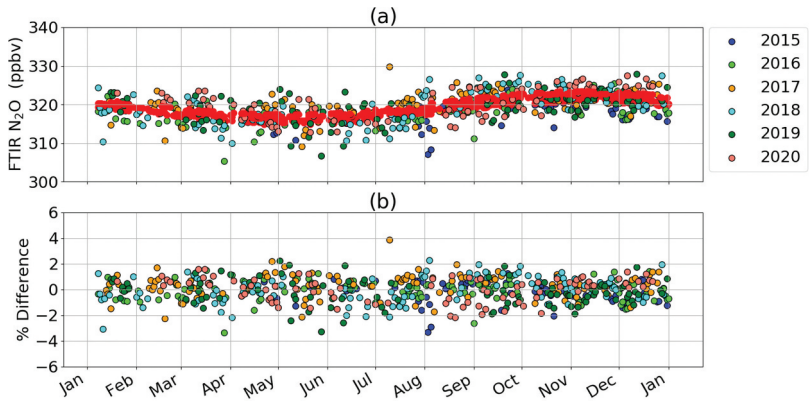

Figure 7. (a) Seasonal variabilities of X_{N_2O} over Hefei based on joint NIR+MIR X_{N_2O} measurements from 2015 to 2020. The red dots represent monthly mean values of X_{N_2O}. (b) Fractional differences of X_{N_2O} measurements relative to the monthly mean values represented by the red dots in (a).

season and observation time, the seasonal X_{N_2O} enhancements spanned a narrow range of −3.89% to 4.05% (Figure 7). The small values of inter-annual trend and seasonal enhancement are mainly attributed to the chemical stable characteristics of N_2O in the atmosphere.

3.3. Comparisons with GEOS-Chem model

GEOS-Chem simulations within ±1 hour of the FTIR measurement times are compared with the joint NIR + MIR observations. Similar to section 3.1, we also use the methodology of Rodgers and Connor (2003) to project the GEOS-Chem model dataset into MIR retrieval scenarios before using them in comparison. The GEOS-Chem simulations sample at the nearest ground pixel to the Hefei site are first vertically interpolated into the MIR vertical height. The interpolated data are then smoothed with the AKs and a priori profiles of MIR retrievals via Equation (10).

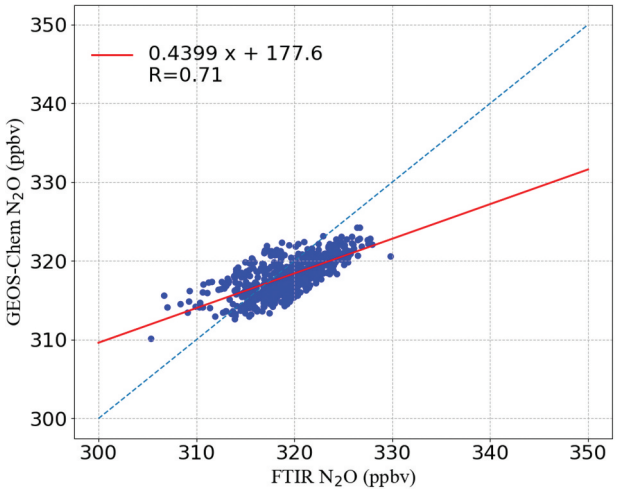

Figure 8. Correlation plots of the joint NIR+MIR data against GEOS-Chem model data. The red line represents a linear fit to the scatter points. The dotted grey line is the 1:1 line.

$$X_s = X_a + \boldsymbol{A}(\boldsymbol{X_c} - \boldsymbol{X_a}), \tag{10}$$

where X_c and X_s are the interpolated and smoothed GEOS-Chem profile, respectively; $\boldsymbol{A}$ and X_a are AK matrix and *a priori* profile of MIR retrievals, respectively. The GEOS-Chem X_{N_2O} is obtained by an integration of the smoothed GEOS-Chem profile from ground to the 120 km.

GEOS-Chem model X_{N_2O} data were generally consistent with FTIR X_{N_2O} data over Hefei, with a correlation of 0.71 (Figure 8). However, GEOS-Chem model data tend to underestimate N_2O concentration and its seasonality in Hefei, especially in autumn and winter (Figure 5). The maximum and minimum values of GEOS-Chem model X_{N_2O} data are (320.17 ± 1.31) ppbv and (315.61 ± 1.52) ppbv in November and March, respectively. Monthly mean differences between FTIR measurements and GEOS-Chem data are within (1.34 ± 3.12) ppbv, where the maximum and minimum differences are (2.65 ± 2.14) ppbv and (0.88 ± 2.05) ppbv in February and June, respectively. The discrepancies between GEOS-Chem simulations and FTIR measurements are mainly attributed to uncertainties of model inputs such as emission inventories and meteorological fields.

4. Conclusions

Both NIR and MIR solar spectra saved by ground-based high resolution FTIR spectrometer were used to retrieve X_{N_2O} over Hefei, eastern China. The X_{N_2O} retrievals derived from NIR and MIR solar spectra were characterized and compared. Generally, NIR and MIR measurements agree well with an R of 0.86 and an average difference of (1.33 ± 4.05) ppbv (NIR – MIR). By reconciling this difference, the joint NIR+MIR observations disclose that the monthly mean time series of X_{N_2O} minimize in June and maximize in September, with values of (316.55 ± 12.22) ppbv and (322.05 ± 12.93) ppbv, respectively. The X_{N_2O} measurements in September were on average (1.71 ± 5.22) % higher than

those in June. The observed X_{N_2O} measurements between 2015 and 2020 showed a positive inter-annual trend of (0.53 ± 0.10) %/year. We also compared GEOS-Chem simulations with the joint NIR+MIR measurements. GEOS-Chem model X_{N_2O} data were generally consistent with FTIR measurement X_{N_2O} data over Hefei, with a correlation coefficient and an average difference of 0.71 and (1.25 ± 4.31) ppbv, respectively. This study can enhance current knowledge of ground-based high-resolution FTIR remote sensing of N_2O in the atmosphere and contribute to generating a new reliable N_2O dataset for climate change research.

Disclosure statement

No potential conflict of interest was reported by the author(s).

Funding

This work is supported by the Youth Innovation Promotion Association, CAS [No. 2019434], National Natural Science Foundation of China [No. U21A2027], the Strategic Priority Research Program of the Chinese Academy of Sciences [No. XDA23020301], the Key Research and Development Project of Anhui Province [No. 202104i07020002], the Major Projects of High Resolution Earth Observation Systems of National Science and Technology [No. 05-Y30B01-9001-19/20-3], and the Sino-German Mobility programme [No. M-0036].

Notes on contributors

Youwen Sun is currently a professor at Anhui Institute of Optics and Fine Mechanics, HFIPS, Chinese Academy of Sciences. He is responsible for the establishment and operation of first internationally recognized high-resolution FTIR remote sensing system in China. His research interests include atmospheric remote sensing, source and sink of atmospheric pollutions/greenhouse gases.

Hao Yin is currently the PhD candidate of University of Science and Technology of China. His current research interests include machine learning, atmospheric remote sensing, atmospheric chemistry and transport model, and spatial data mining.

Wei Wang is currently a professor at Anhui Institute of Optics and Fine Mechanics, HFIPS, Chinese Academy of Sciences. She is responsible for the establishment and operation of the first internationally recognized high-resolution FTIR remote sensing system in China. Her research interests include atmospheric remote sensing and environmental optics.

Changgong Shan is currently an assistant professor at Anhui Institute of Optics and Fine Mechanics, HFIPS, Chinese Academy of Sciences. He participated in the establishment and operation of the first internationally recognized high-resolution FTIR remote sensing system in China. His research interests include atmospheric remote sensing and environmental optics.

Cheng Liu is currently a professor at University of Science and Technology of China. He developed a variety of satellite remote sensing retrieval algorithms for atmospheric trace gas. He is the PI of the first internationally recognized high-resolution FTIR remote sensing system in China. His research interests include atmospheric remote sensing, spatial data mining, and environmental optics.

ORCID

Youwen Sun http://orcid.org/0000-0003-3126-3252
Hao Yin http://orcid.org/0000-0002-4399-5752

Data availability statement

Data underlying the results presented in this paper are not publicly available at this time but may be obtained from the authors upon reasonable request.

References

Addington, O., Z. Zeng, T. Pongetti, R. Shia, K. R. Gurney, J. Liang, G. Roest, L. He, Y. L. Yung, and S. P. Sander. 2021. "Estimating Nitrous Oxide (N_2O) Emissions for the Los Angeles Megacity Using Mountaintop Remote Sensing Observations." *Remote Sensing of Environment* 259: 112351. doi:10.1016/j.rse.2021.112351.

Angelbratt, J., J. Mellqvist, T. Blumenstock, T. Borsdorff, S. Brohede, P. Duchatelet, F. Forster, et al. 2011. "A New Method to Detect Long Term Trends of Methane (CH_4) and Nitrous Oxide (N_2O) Total Columns Measured Within the NDACC Ground-Based High Resolution Solar FTIR Network." *Atmospheric Chemistry and Physics* 11 (13): 6167–6183. doi:10.5194/acp-11-6167-2011.

Eastham, S. D., D. K. Weisenstein, and S. R. H. Barrett. 2014. "Development and Evaluation of the Unified Tropospheric–Stratospheric Chemistry Extension (UCX) for the Global Chemistry-Transport Model GEOS-Chem." *Atmospheric Environment* 89: 52–63. doi:10.1016/j.atmosenv.2014.02.001.

Giglio, L., J. T. Randerson, and G. R. Van Der Werf. 2013. "Analysis of Daily, Monthly, and Annual Burned Area Using the Fourth-Generation Global Fire Emissions Database (GFED4)." *Journal of Geophysical Research-Biogeosciences* 118 (1): 317–328. doi:10.1002/jgrg.20042.

Hall, B. D., G. S. Dutton, D. J. Mondeel, J. D. Nance, M. Rigby, J. H. Butler, F. L. Moore, D. F. Hurst, and J. W. Elkins. 2011. "Improving Measurements of SF_6 for the Study of Atmospheric Transport and Emissions." *Atmospheric Measurement Techniques* 4 (11): 2441–2451. doi:10.5194/amt-4-2441-2011.

Hase, F. 2012. "Improved Instrumental Line Shape Monitoring for the Ground-Based, High-Resolution FTIR Spectrometers of the Network for the Detection of Atmospheric Composition Change." *Atmospheric Measurement Techniques* 5 (3): 603–610. doi:10.5194/amt-5-603-2012.

Hase, F., T. Blumenstock, and C. Paton-Walsh. 1999. "Analysis of the Instrumental Line Shape of High-Resolution Fourier Transform IR Spectrometers with Gas Cell Measurements and New Retrieval Software." *Applied Optics* 38 (15): 3417–3422. doi:10.1364/AO.38.003417.

Hill, C., I. E. Gordon, L. S. Rothman, and J. Tennyson. 2013. "A New Relational Database Structure and Online Interface for the HITRAN Database." *Journal of*

Quantitative Spectroscopy & Radiative Transfer 130: 51–61. doi:10.1016/j.jqsrt.2013.04.027.

Hoesly, R. M., S. J. Smith, L. Y. Feng, Z. Klimont, G. Janssens-Maenhout, T. Pitkanen, J. J. Seibert, et al. 2018. "Historical (1750–2014) Anthropogenic Emissions of Reactive Gases and Aerosols from the Community Emissions Data System (CEDS)." *Geoscientific Model Development* 11 (1): 369–408. doi:10.5194/gmd-11-369-2018.

Kalnay, E., M. Kanamitsu, R. Kistler, W. Collins, D. Deaven, L. Gandin, M. Iredell, et al. 1996. "The NCEP/NCAR 40-Year Reanalysis Project." *Bulletin of the American Meteorological Society* 77 (3): 437–472. doi:10.1175/1520-0477(1996)077<0437:TNYRP>2.0.CO;2.

Machida, T., T. Nakazawa, Y. Fujii, S. Aoki, and O. Watanabe. 1995. "Increase in the Atmospheric Nitrous Oxide Concentration During the Last 250 Years." *Geophysical Research Letters* 22 (21): 2921–2924. doi:10.1029/95GL02822.

Mclinden, C. A., S. C. Olsen, B. Hannegan, O. Wild, M. J. Prather, and J. Sundet. 2000. "Stratospheric Ozone in 3-D Models: A Simple Chemistry and the Cross-Tropopause Flux." *Journal of Geophysical Research Atmospheres* 105 (D11): 14653–14665. doi:10.1029/2000JD900124.

Montzka, S. A., E. J. Dlugokencky, and J. H. Butler. 2011. "Non-CO_2 Greenhouse Gases and Climate Change." *Nature* 476 (7358): 43–50. doi:10.1038/nature10322.

Morgan, C. G., M. Allen, M. C. Liang, R. L. Shia, G. A. Blake, and Y. L. Yung. 2004. "Isotopic Fractionation of Nitrous Oxide in the Stratosphere: Comparison Between Model and Observations." *Journal of Geophysical Research Atmospheres* 109 (D4). doi:10.1029/2003JD003402.

Murray, L. T., D. J. Jacob, J. A. Logan, R. C. Hudman, and W. J. Koshak. 2012. "Optimized Regional and Interannual Variability of Lightning in a Global Chemical Transport Model Constrained by LIS/OTD Satellite Data." *Journal of Geophysical Research Atmospheres* 117 (D20). doi:10.1029/2012JD017934.

Nevison, C. D., E. Dlugokencky, G. Dutton, J. W. Elkins, P. Fraser, B. Hall, and P. B. Krummel. 2011. "Exploring Causes of Interannual Variability in the Seasonal Cycles of Tropospheric Nitrous Oxide." *Atmospheric Chemistry and Physics* 11 (8): 3713–3730.

Parrish, D. D., J. F. Lamarque, V. Naik, L. Horowitz, D. T. Shindell, J. Staehelin, R. Derwent, et al. 2014. "Long-Term Changes in Lower Tropospheric Baseline Ozone Concentrations: Comparing Chemistry-Climate Models and Observations at Northern Midlatitudes." *Journal of Geophysical Research Atmospheres* 119 (9): 5719–5736. doi:10.1002/2013JD021435.

Portmann, R. W., J. S. Daniel, and A. R. Ravishankara. 2012. "Stratospheric Ozone Depletion Due to Nitrous Oxide: Influences of Other Gases." *Philosophical Transactions of the Royal Society B: Biological Sciences* 367 (1593): 1256–1264. doi:10.1098/rstb.2011.0377.

Prinn, R., D. Cunnold, R. Rasmussen, P. Simmonds, F. Alyea, A. Crawford, P. Fraser, and R. Rosen. 1990. "Atmospheric Emissions and Trends of Nitrous Oxide Deduced from 10 Years of ALE–GAGE Data." *Journal of Geophysical Research Atmospheres* 95 (D11): 18369–18385. doi:10.1029/JD095iD11p18369.

Prinn, R. G., R. F. Weiss, P. J. Fraser, P. G. Simmonds, D. M. Cunnold, F. N. Alyea, S. O'doherty, et al. 2000. "A History of Chemically and Radiatively Important Gases in Air Deduced from ALE/GAGE/AGAGE." *Journal of Geophysical Research Atmospheres* 105 (D14): 17751–17792. doi:10.1029/2000JD900141.

Ravishankara, A. R., J. Daniel, and R. Portmann. 2009. "Nitrous Oxide (N2O): The Dominant Ozone-Depleting Substance Emitted in the 21st Century." *Science* 326 (5949): 123–125. doi:10.1126/science.1176985.

Rodgers, C. 2000. *Inverse Methods for Atmospheric Sounding - Theory and Practice*. Singapore: World Scientific.

Rodgers, C. D., and B. J. Connor. 2003. "Intercomparison of Remote Sounding Instruments." *Journal of Geophysical Research-Atmospheres* 108 (D3). doi:10.1029/2002JD002299.

Rothman, L. S., I. E. Gordon, A. Barbe, D. C. Benner, P. F. Bernath, M. Birk, V. Boudon, et al. 2009. "The HITRAN 2008 Molecular Spectroscopic Database." *Journal of Quantitative Spectroscopy & Radiative Transfer* 110 (9): 533–572. doi:10.1016/j.jqsrt.2009.02.013.

Sagar, V. K., M. Pathakoti, D. V. Mahalakshmi, K. S. Rajan, M. V. R. S. Sesha, F. Hase, D. Dubravica, and M. K. Sha. 2022. "Ground-Based Remote Sensing of Total Columnar CO_2, CH_4, and CO Using EM27/SUN FTIR Spectrometer at a Suburban Location (Shadnagar) in India and Validation of Sentinel-5P/TROPOMI." *IEEE Geoscience and Remote Sensing Letters* 19: 1–5. doi:10.1109/LGRS.2022.3171216.

Stein, L. Y., and Y. L. Yung. 2003. "Production, Isotopic Composition, and Atmospheric Fate of Biologically Produced Nitrous Oxide." *Annual Review of Earth and Planetary Sciences* 31 (1): 329–356. doi:10.1146/annurev.earth.31.110502.080901.

Sun, Y., C. Liu, L. Zhang, M. Palm, J. Notholt, H. Yin, C. Vigouroux, et al. 2020. "Fourier Transform Infrared Time Series of Tropospheric HCN in Eastern China: Seasonality, Interannual Variability, and Source Attribution." *Atmospheric Chemistry and Physics* 20 (9): 5437–5456. doi:10.5194/acp-20-5437-2020.

Sun, Y., M. Palm, C. Liu, F. Hase, D. Griffith, C. Weinzierl, C. Petri, W. Wang, and J. Notholt. 2018a. "The Influence of Instrumental Line Shape Degradation on Ndacc Gas Retrievals: Total Column and Profile." *Atmospheric Measurement Techniques* 11 (5): 2879–2896. doi:10.5194/amt-11-2879-2018.

Sun, Y., M. Palm, C. Liu, F. Hase, D. Griffith, C. Weinzierl, C. Petri, W. Wang, and J. Notholt. 2018b. "The Influence of Instrumental Line Shape Degradation on Ndacc Gas Retrievals: Total Column and Profile." *Atmospheric Measurement Techniques* 11 (5): 2879–2896. doi:10.5194/amt-11-2879-2018.

Sun, Y., M. Palm, C. Weinzierl, C. Petri, J. Notholt, Y. Wang, and C. Liu. 2017. "Technical Note: Sensitivity of Instrumental Line Shape Monitoring for the Ground-Based High-Resolution Ftir Spectrometer with Respect to Different Optical Attenuators." *Atmospheric Measurement Techniques* 10 (3): 989–997. doi:10.5194/amt-10-989-2017.

Sun, Y., H. Yin, Y. Cheng, Q. Zhang, B. Zheng, J. Notholt, X. Lu, C. Liu, Y. Tian, and J. Liu. 2021c. "Quantifying Variability, Source, and Transport of CO in the Urban Areas Over the Himalayas and Tibetan Plateau." *Atmospheric Chemistry and Physics* 21 (11): 9201–9222. doi:10.5194/acp-21-9201-2021.

Sun, Y., H. Yin, C. Liu, E. Mahieu, J. Notholt, Y. Té, X. Lu, et al. 2021a. "The Reduction in C_2H_6 from 2015 to 2020 Over Hefei, Eastern China, Points to Air Quality Improvement in China." *Atmospheric Chemistry and Physics* 21 (15): 11759–11779. doi:10.5194/acp-21-11759-2021.

Sun, Y., H. Yin, C. Liu, L. Zhang, Y. Cheng, M. Palm, J. Notholt, et al. 2021b. "Mapping the Drivers of Formaldehyde (HCHO) Variability from 2015 to 2019 Over Eastern China: Insights from Fourier Transform Infrared Observation and Geos-Chem Model Simulation." *Atmospheric Chemistry and Physics* 21 (8): 6365–6387. doi:10.5194/acp-21-6365-2021.

Tian, Y., Y. Sun, C. Liu, W. Wang, C. Shan, X. Xu, and Q. Hu. 2017. "Characterisation of Methane Variability and Trends from Near-Infrared Solar Spectra Over Hefei, China." *Atmospheric Environment* 173: 198–209. doi:10.1016/j.atmosenv.2017.11.001.

UNFCC (United Nations Framework Convention on Climate Change). 1997. "Kyoto Protocol to the United Nations Framework Convention on Climate Change." Accessed December 20 2022. https://unfccc.int/kyoto.protocol

United States Environmental Protection Agency. 2019. "Overview of Greenhouse Gases." Accessed December 20 2022. epa.gov/ghgemissions/overview-greenhouse-gases

Wang, W., Y. Tian, C. Liu, Y. Sun, W. Liu, P. Xie, J. Liu, et al. 2017. "Investigating the Performance of a Greenhouse Gas Observatory in Hefei, China." *Atmospheric Measurement Techniques* 10 (7): 2627–2643. doi:10.5194/amt-10-2627-2017.

Wunch, D., G. C. Toon, J. F. L. Blavier, R. A. Washenfelder, J. Notholt, B. J. Connor, D. W. T. Griffith, V. Sherlock, and P. O. Wennberg. 2011. "The Total Carbon Column Observing Network." *Philosophical Transactions of the Royal Society A-Mathematical Physical and Engineering Sciences* 369 (1943): 2087–2112. doi:10.1098/rsta.2010.0240.

Wunch, D., G. C. Toon, V. Sherlock, N. M. Deutscher, X. Liu, D. G. Feist, and P. O. Wennberg. 2015. "The Total Carbon Column Observing Network's GGG2014 Data Version." Accessed December 20 2022. https://tccon-data.org/2014

Yang, Y., M. Zhou, B. Langerock, M. K. Sha, C. Hermans, T. Wang, D. Ji, et al. 2020. "New Ground-Based Fourier-Transform Near-Infrared Solar Absorption Measurements of XCO_2, XCH_4 and XCO at Xianghe, China." *Earth System Science Data* 12 (3): 1679–1696. doi:10.5194/essd-12-1679-2020.

Yin, H., Y. Sun, C. Liu, X. Lu, D. Smale, T. Blumenstock, T. Nagahama, et al. 2020. "Ground-Based Ftir Observation of Hydrogen Chloride (HCl) Over Hefei, China, and Comparisons with Geos-Chem Model Data and Other Ground-Based Ftir Stations Data." *Optics Express* 28 (6): 8041–8055. doi:10.1364/OE.384377.

Yin, H., Y. Sun, C. Liu, W. Wang, C. Shan, and L. Zha. 2021a. "Remote Sensing of Atmospheric Hydrogen Fluoride (HF) Over Hefei, China with Ground-Based High-Resolution Fourier Transform Infrared (FTIR) Spectrometry." *Remote Sensing* 13 (4): 791. doi:10.3390/rs13040791.

Yin, H., Y. Sun, C. Liu, L. Zhang, X. Lu, W. Wang, C. Shan, et al. 2019. "First Time Series of Stratospheric NO_2 Over Hefei, China, and Comparisons with Omi and Geos-Chem Model Data." *Optics Express* 27 (16): A1225–1240. doi:10.1364/OE.27.0A1225.

Yin, H., Y. Sun, J. Notholt, M. Palm, and C. Liu. 2022a. "Spaceborne Tropospheric Nitrogen Dioxide (NO_2) Observations from 2005–2020 Over the Yangtze River Delta (Yrd), China: Variabilities, Implications, and Drivers." *Atmospheric Chemistry and Physics* 22 (6): 4167–4185. doi:10.5194/acp-22-4167-2022.

Yin, H., Y. Sun, W. Wang, C. Shan, Y. Tian, and C. Liu. 2021b. "Ground-Based High-Resolution Remote Sensing of Sulphur Hexafluoride (SF_6) Over Hefei, China: Characterization, Optical Misalignment, Influence, and Variability." *Optics Express* 29 (21): 34051–34065. doi:10.1364/OE.440193.

Yin, H., Y. Sun, Y. You, J. Notholt, M. Palm, W. Wang, C. Shan, and C. Liu. 2022b. "Using Machine Learning Approach to Reproduce the Measured Feature and Understand the Model-To-Measurement Discrepancy of Atmospheric Formaldehyde." *The Science of the Total Environment* 851: 158271. doi:10.1016/j.scitotenv.2022.158271.

Zhou, M., B. Langerock, K. C. Wells, D. B. Millet, C. Vigouroux, M. K. Sha, C. Hermans, et al. 2019. "An Intercomparison of Total Column-Averaged Nitrous Oxide Between Ground-Based FTIR TCCON and NDACC Measurements at Seven Sites and Comparisons with the Geos-Chem Model." *Atmospheric Measurement Techniques* 12 (2): 1393–1408. doi:10.5194/amt-12-1393-2019.